Original Article

MOLECULAR METABOLISM

Serum amyloid A1 exacerbates hepatic steatosis via TLR4-mediated NF-κB signaling pathway

Bin Jiang [1,4], Dongdong Wang [1,4], Yunfu Hu [1], Wenxuan Li [1], Fengjiang Liu [3], Xudong Zhu [1], Xiaoyu Li [1], Hanwen Zhang [1], Hui Bai [1], Qing Yang [1], Xiuna Yang [2,*], Jingjing Ben [1,**], Qi Chen [1,*]**

ABSTRACT

Objective: Chronic inflammatory response plays a prominent role in obesity-related nonalcoholic fatty liver disease (NAFLD). However, the intrahepatic triggering mechanism of inflammation remains obscure. This study aimed to elucidate the role of serum amyloid A1 (SAA1), an acute-phase response protein, in the obesity-induced hepatic inflammation and NAFLD.

Methods: Male mice were fed a high fat diet (HFD) for 16 weeks, and insulin resistance, hepatic steatosis, and inflammation in mice were monitored. Murine SAA1/2 was genetically manipulated to investigate the role of SAA1 in NAFLD.

Results: We found that SAA1 was increased in the NAFLD liver in both humans and mice. Knockout of SAA1/2 or knockdown of hepatic SAA1/2 promoted energy expenditure and alleviated HFD-induced metabolic disorder, hepatic steatosis, and inflammation. Endogenous overexpression of SAA1 in hepatocytes by adeno-associated virus 8 (AAV8) transfection aggravated overnutrition-associated gain of body weight, insulin resistance, hepatic lipid accumulation, and liver injury, which were markedly alleviated by knockout of murine toll-like receptor 4 (TLR4). Mechanistically, SAA1 directly bound with TLR4/myeloid differentiation 2 (MD2) to induce TLR4 internalization, leading to the activation of nuclear factor (NF)-κB signaling and production of both SAA1 and other inflammatory cytokines, including interleukin (IL)-6 and C—C chemokine ligand (CCL2) in hepatocytes. Administration of HFD mice with an AAV8-shRNA-*SAA1/2* showed a therapeutic effect on hepatic inflammation and NAFLD progression.

Conclusions: These results demonstrate that SAA1 triggers hepatic steatosis and intrahepatic inflammatory response by forming a SAA1/TLR4/NF-κB/SAA1 feedforward regulatory circuit, which, in turn, leads to NAFLD progression. SAA1 may act as a potential target for the disease intervention.

Keywords Hepatic steatosis; Non-alcoholic fatty liver disease; NF-κB signaling pathway; Obesity; Serum amyloid A1; Toll-like receptor

1. INTRODUCTION

Nonalcoholic fatty liver disease (NAFLD), termed as metabolic-associated fatty liver disease (MAFLD) recently [1], is thought a global health crisis that is closely associated with obesity, insulin resistance, and hyperlipidemia [2]. The spectrum of NAFLD ranges from simple steatosis to the potentially progressive nonalcoholic steatohepatitis (NASH), of which adverse hepatic outcomes include dysfunctional fibrosis, cirrhosis, and hepatocellular carcinoma (HCC) [3,4]. However, there is currently no effective therapy available for the treatment of NAFLD [5]. Pathogenesis of NAFLD is very complex involving many pathological processes. When the primary metabolic energy substrates, namely carbohydrates and fatty acids, exceed the handling capacity of the liver, the toxic lipid species may accumulate in the liver, leading to hepatocellular stress, injury, and death [4,6]. Besides, overnutrition triggers liver inflammation by both extrahepatic (such as in adipose tissue and gut) and intrahepatic (for example, lipotoxicity, innate immune response, and cell death pathways) mechanisms in a parallel or sequential fashion [7]. The concerted and differential action of inflammatory responses determines the clinical and histological phenotypes of the disease, leading to fibrogenesis and genomic instability that predispose to cirrhosis and hepatocellular carcinoma. For example, the endotoxins and metabolic damage induce inflammatory responses by activating toll-like receptor 4 (TLR4), thereby facilitating the progression of hepatic steatosis to NASH and HCC [8,9]. However, the translative relevance of inflammation in NAFLD remains challenging. Deep insight into the regulatory mechanism of inflammation helps to generate novel therapies for the treatment of NAFLD.

Serum amyloid A (SAA) is a family of differentially expressed apolipoproteins comprising several isoforms, including SAA1, SAA2, and

[1]Department of Pathophysiology, Key Laboratory of Cardiovascular Disease and Molecular Intervention, Nanjing Medical University, Nanjing, China [2]Institute for Advanced Immunochemical Studies, ShanghaiTech University, Shanghai, China [3]Innovative Center for Pathogen Research, Guangzhou Laboratory, Guangzhou, China

[4] Bin Jiang and Dongdong Wang contributed equally to this work.

*Corresponding author. E-mail: qichen@njmu.edu.cn (Q. Chen).

***Corresponding author. E-mail: yangxn@shanghaitech.edu.cn (X. Yang).

**Corresponding author. E-mail: bjj@njmu.edu.cn (J. Ben).

Received October 27, 2021 • Revision received February 10, 2022 • Accepted February 10, 2022 • Available online 3 March 2022

https://doi.org/10.1016/j.molmet.2022.101462

SAA4. SAA1 and SAA2 isoforms are highly homologous and mainly expressed in hepatocytes. The serum level of SAA is normally quite low, but it can rise sharply after the onset of acute phase response resulted from inflammation, infection, trauma, and cancer [10,11]. As an acute phase protein, SAA1 has been reported to involve type 2 diabetes in human study [12]. SAA1 knockdown alleviates obesity and insulin resistance via inhibiting nuclear factor (NF)-κB signaling [13,14]. Patients with NAFLD have elevated levels of serum SAA1 [15,16]. SAA1 can promote platelet aggregation and inflammatory cell recruitment to the liver in high fat diet (HFD)-fed mice [17]. In addition, SAA1 has a stimulative effect on the production of interleukin (IL)-17, IL-1β and C—C chemokine ligand 2 (CCL2) [18—20]. These findings bridge relation of SAA1 to toxic lipid accumulation and pathogenic inflammation in the progression of NAFLD. However, the exact role of SAA1 in NAFLD and the mechanism by which SAA1 induces hepatic inflammation urgently need to be elucidated, which will help to understand the transition from nonalcoholic fatty liver to NASH.

Here, we report that knockout of SAA1/2 or knockdown of SAA1/2 prevented the development of hepatic steatosis and inflammation in mice. Mechanistic studies reveal that SAA1 aggravated hepatic inflammation by directly binding with TLR4 and myeloid differentiation 2 (MD2) and triggering TLR4 internalization, thereby activating NF-κB signaling and, in turn, boosting the production of SAA1. The SAA1/TLR4/NF-κB/SAA1 feedforward regulatory circuit may contribute to inflammation in the liver that would be a potential target for NAFLD intervention.

2. MATERIALS AND METHODS

2.1. Human liver samples

Liver samples for immunohistochemical (IHC) analysis from 30 patients were obtained either by liver biopsy for diagnostic purposes or from surgical liver resections at Nanjing Medical University First Affiliated Hospital. Accordingly, liver samples from individuals with excessive alcohol consumption (>140 g for men or >70 g for women, per week), drug abuse or viral infection (e.g., hepatitis B virus and hepatitis C virus) were excluded [21]. Each patient provided informed consent for the analysis of tissues, which were subjected to paraffin embedding. Histological slides were assessed and scored by a pathologist. The severity level of fatty liver was graded into simple, mild, and severe according to the American Association for the Study of Liver Diseases guideline [22]. Cases with NAFLD activity scores (NAS) of 1—2, ballooning scores of 0 and no fibrosis were classified as simple steatosis. Cases with NAS of 3—4 but with fibrosis were classified as mild steatosis, and those with NAS ≥5 were classified as severe steatosis. All procedures involved human liver samples in this study were approved by the Ethics Committee of Nanjing Medical University First Affiliated Hospital and adhered to the principles of the Declaration of Helsinki. The clinical data of all subjects are summarized in Supplementary Table 1.

2.2. Mice

Knockout of SAA1/2 in C57BL/6J mice was generated by the CRISPR/Cas9 approach. Two single-guide RNAs (sgRNAs)-targeting exons on both sides of the targeted region of SAA1 and SAA2 were respectively constructed and transcribed *in vitro*. The primers used for the knockout and identification are listed in Supplementary Table 2. Cas9 mRNA and sgRNA were co-injected into zygotes, and the zygotes were then transferred into the oviduct of pseudo pregnant ICR females at 0.5 dpc. The F0 mice were birthed after 19—21 days of transplantation. All tail DNA of F0 off springs were sequenced by PCR. The F0 mice were crossed with C57BL/6J mice to build up heterozygous mice, which interbred with each other to obtain SAA1/2 knockout homozygous (*SAA1/2*$^{-/-}$) mice. The *SAA1/2*$^{-/-}$ mice were born with normal Mendelian ratios. To identify the efficiency of SAA1/2 knockout, an acute phase response was elicited by an intraperitoneal injection of 1 μg g^{-1} lipopolysaccharide (LPS, L4516, Sigma—Aldrich) into male *SAA1/2*$^{-/-}$ mice and WT mice. After 24 h, the mice were humanely euthanized, and the livers and plasma were collected for SAA1/2 analysis.

Male *TLR4*$^{-/-}$ ([Tlr4$^{lps\text{-}del}$] mut/mut, C57BL/10ScNJNju) mice, and control mice (C57BL/10JNju) were purchased from the Model Animal Research Center of Nanjing University (Nanjing, China).

The fatty liver model was established in 7- to 8-week-old male mice by feeding a HFD (D12492, Research Diets) for 16 weeks or a Western diet (WD, D12079B, Research Diets) for 8 weeks. Mice fed chow diet (CD) served as controls. Body weight and blood glucose were measured weekly after 6 h of fasting. Blood samples were obtained from the tail vein for measuring glucose levels by a handheld glucometer (One Touch Horizon Glucose Monitoring kit, LifeScan).

To generate mice with overexpression of SAA1 in the liver, the reconstructed adeno-associated virus 8 encoding *SAA1* gene (AAV8-SAA1, Shanghai Genechem Co., Ltd.) was injected via the tail vein into 8-week-old male *TLR4*$^{-/-}$ and control mice (4×10^{11} viral particles/mouse). AAV8-green fluorescent protein (GFP) was used as controls (AAV8-Control). After 3 days, mice were fed a HFD for 16 weeks.

To knock down hepatic SAA1/2, the AAV8 encoding SAA1/2-specific short hairpin (sh) RNA (AAV8-shRNA-*SAA1/2*: 5′-GCGAGCCTA-CACTGACATGAA-3′, Shandong WZ Biosciences Co., Ltd.) was intravenously injected into adult male C57BL/6J mice. The AAV8-shRNA-scramble (AAV8-shRNA-sc) was used as a nontargeting control. Each mouse was injected with 2.5×10^{11} viral particles and then fed a HFD for 16 weeks. For the therapeutic experiments, male C57BL/6J mice fed a HFD for 6 weeks were injected by AAV8-shRNA-*SAA1/2* or AAV8-shRNA-sc and then fed a HFD for another 10 weeks. Mice were maintained in a standard environment with a 12 h-light—dark cycle and were allowed free access to water and food. All animal procedures were performed in accordance with protocols approved by the Institutional Animal Care and Usage Committee of Nanjing Medical university.

2.3. Cell culture

Primary hepatocytes from 4- to 6-week-old male C57BL/6J mice were isolated as described previously [21]. HEK293T cells used in this study were purchased from the Type Culture Collection of the Chinese Academy of Sciences (Shanghai, China). HEK293T cells were cultured in DMEM supplemented with 10% FBS and 1% P/S in a 5% CO_2 humidified atmosphere.

2.4. Protein expression

Mouse SAA1 (residues 19—122) was cloned into the pET30(a)$^{+}$ expression vector between *Nde*I and *Hin*dIII restriction endonuclease sites, with a N-terminal hexa-histidine and subsequently transformed into BL21 (DE3) strain of *Escherichia coli*. The culture was grown in terrific broth medium to an optical density at 0.6 OD at 37 °C and induced with 1 mM isopropyl-β-D-galactoside (IPTG, I6758, Sigma—Aldrich) for 4 h at 25 °C. Proteins were purified following the previously published protocol [18]. Briefly, cells were harvested and re-suspended in lysis buffer (50 mM Tris pH 8.0, 500 mM NaCl, 10 mM imidizole). After sonication and centrifugation at 12,000 *g* for 30 min, 40 mM decyl maltopyranoside (DM, D322, Avanti Polar Lipids)

was added to the suspension and incubated for 3 h at 4 °C. After centrifugation, the suspension was incubated with Ni-NTA resin (Qiagen) and eluted. Gel-filtration chromatography was used for further purification, and protein purity was assessed by SDS-PAGE. The mouse SAA1 protein was treated by Triton X-114 to remove endotoxin. Endotoxin in the recombinant SAA1 was less than 0.5 EU/ml of protein. Recombinant mouse TLR4 and MD2 were prepared as described previously [23]. Briefly, the ectodomain of mouse TLR4 (residues 22—627) and the mouse MD2 (residues 19—160) fused to the Protein A tag were co-expressed in High Five insect cells and purified by IgG Sepharose affinity chromatography (GE Healthcare Life Sciences). The protein A tag was cleared by human rhinovirus 3C protease. The mTLR4-MD2 complex was subjected to gel filtration chromatography with Superdex 200 column (GE Healthcare Life Sciences).

2.5. Intraperitoneal glucose and insulin tolerance measurements

Intraperitoneal glucose and insulin tolerance were determined as described previously [24]. For glucose tolerance tests, mice were intraperitoneally injected with glucose solution (1.5 g kg^{-1}) after 16 h of fasting. For insulin tolerance tests, human regular insulin (1 U kg^{-1}) was intraperitoneally injected after 6 h of fasting. Blood glucose levels were examined at the indicated time points.

2.6. Analysis of metabolic parameters and liver function

At the end of HFD feeding, mice were anaesthetized by an intraperitoneal injection of a xylazine and ketamine mixture (10 mg kg^{-1} and 100 mg kg^{-1}, respectively) after 6 h of fasting, and blood was sampled. Mice were euthanized by CO_2 inhalation, and the tissues were collected for subsequent experiments. Non-esterified fatty acid (NEFA), triglycerides (TG), total cholesterol (TCH), aspartate aminotransferase (AST) and alanine aminotransferase (ALT) were measured using the indicated enzymatic assays according to the manufacturer's instructions (Jiancheng Bio, China). Plasma levels of IL-1β (R&D system, MLB00C), IL-6 (Multi Sciences, EK206/3—96), tumor necrosis factor (TNF)-α (eBioscience, BMS607-3), CCL2 (eBioscience, BMS6005) and C-reactive protein (CRP) (Multi Sciences, EK294/2—96) were examined by ELISA according to the manufacturer's instructions. For insulin ELISA, plasma was collected from 6-h fasted mice, and the insulin level was determined with a mouse insulin ELISA kit (10-1247-01, Mercodia, Sweden).

2.7. Indirect calorimetry system

Indirect calorimetry was performed by a TSE Phenomaster monitoring system (Phenomaster, TSE Systems GmbH, Germany). For the measurement of food intake and energy expenditure, mice were single housed 3 days prior to the experiment for acclimation. Individual mouse data from the 2 days were averaged and used for the analysis.

2.8. Histological analysis and immunohistochemistry staining

Liver sections were fixed in 4% paraformaldehyde and embedded in paraffin, and then routinely stained with hematoxylin and eosin (H&E) to evaluate hepatic morphology. For visualize the lipid droplet accumulation in the liver, frozen liver sections prepared in Tissue-Tek OCT compound (4583, Sakura Finetek) were stained with Oil Red O (O0625, Sigma—Aldrich).

For IHC staining, liver sections were fixed in 4% paraformaldehyde and embedded in paraffin. After antigen retrieval, the sections were incubated with primary antibodies at 4 °C overnight. Then, the slides were incubated with indicated secondary antibodies conjugated with horseradish peroxidase for 1 h. IHC staining was visualized using DAB according to the manufacturer's instructions.

2.9. Surface plasmon resonance (SPR) experiments

The binding affinity of mouse SAA1 to MD2 or TLR4 was determined by surface plasmon resonance measurements using a BIAcore S200 instrument (GE healthcare). Mouse SAA1 were prepared as mentioned above. Mouse TLR4 was purchased from R&D system, and mouse MD2 was purchased from Beijing ABIOCENTER Co., Ltd. For the binding affinity of mouse SAA1 to MD2, SAA1 was immobilized on the sensor surface. Different concentrations of MD2 were allowed to run sequentially over the immobilized SAA1 to monitor the functionality of the protein surface. For the binding affinity of mSAA1 to mTLR4, TLR4 was immobilized on the sensor surface. Different concentrations of SAA1 were injected over the immobilized TLR4 and reference surface with at least 30 s association and dissociation times. Surface regeneration was achieved using dissociation for a time period allowing the response to return to baseline. SPR equilibrium binding data, consisting of Req values from 6-point concentration series, were analyzed by fitting a steady model to yield Rmax and Kd values using BIAcore S200 Evaluation Software.

2.10. Flow cytometry to determine TLR4 endocytosis

TLR4 endocytosis was determined as described [25]. Briefly, primary mouse hepatocytes were treated with SAA1 (2 μg ml^{-1}) or control for 120 min at 37 °C. Cells were subsequently stained with the antibody against TLR4 (TLR4-APC, SA15-21, BioLegend) for 30 min on ice. The cells marked by the antibody were washed three times with PBS and analyzed with FACS Verse (BD Biosciences). The geometric mean fluorescence intensity of TLR4-APC was recorded.

2.11. Size exclusion chromatography

The dimerization of TLR4-MD2 induced by different ligands was determined as described [26]. The purified mouse TLR4-MD2 complex was incubated with LPS (L9641, Sigma—Aldrich) or mouse SAA1 in room temperature for 30 min. After the reaction, the mixture of TLR4-MD2-LPS or SAA1 complex was applied to Superdex 200 for gel filtration chromatography. The peak elution fractions were analyzed by SDS-PAGE followed by Coomassie brilliant blue staining or gradient Native PAGE gel (4—15%).

2.12. Co-immunoprecipitation and western blot analysis

Co-immunoprecipitation (co-IP) and western blot were performed as described previously [24]. The blots were quantified by Image J Software and normalized to levels of GAPDH. The sources of antibodies used are listed in Supplementary Table 3.

2.13. Quantitative real-time PCR (qRT-PCR)

Total RNAs were extracted from liver tissues or cultured primary mouse hepatocytes using RNAiso Plus (TaKaRa, Japan) and subjected to complementary DNA synthesis using commercial kits (Vazyme Biotech, China) according to the manufacturer's instructions. Gene expression was normalized to the housekeeping gene GAPDH. qRT-PCR primers used in this study are listed in Supplementary Table 2.

2.14. Statistical analysis

Data were analyzed using GraphPad Prism 8.0 software and presented as mean ± standard error of the mean (SEM). Comparisons of two groups were performed by Student's t-test, and comparisons among multiple groups were performed using ANOVA followed by Bonferroni's post hoc test. P values of less than 0.05 were considered statistically significant.

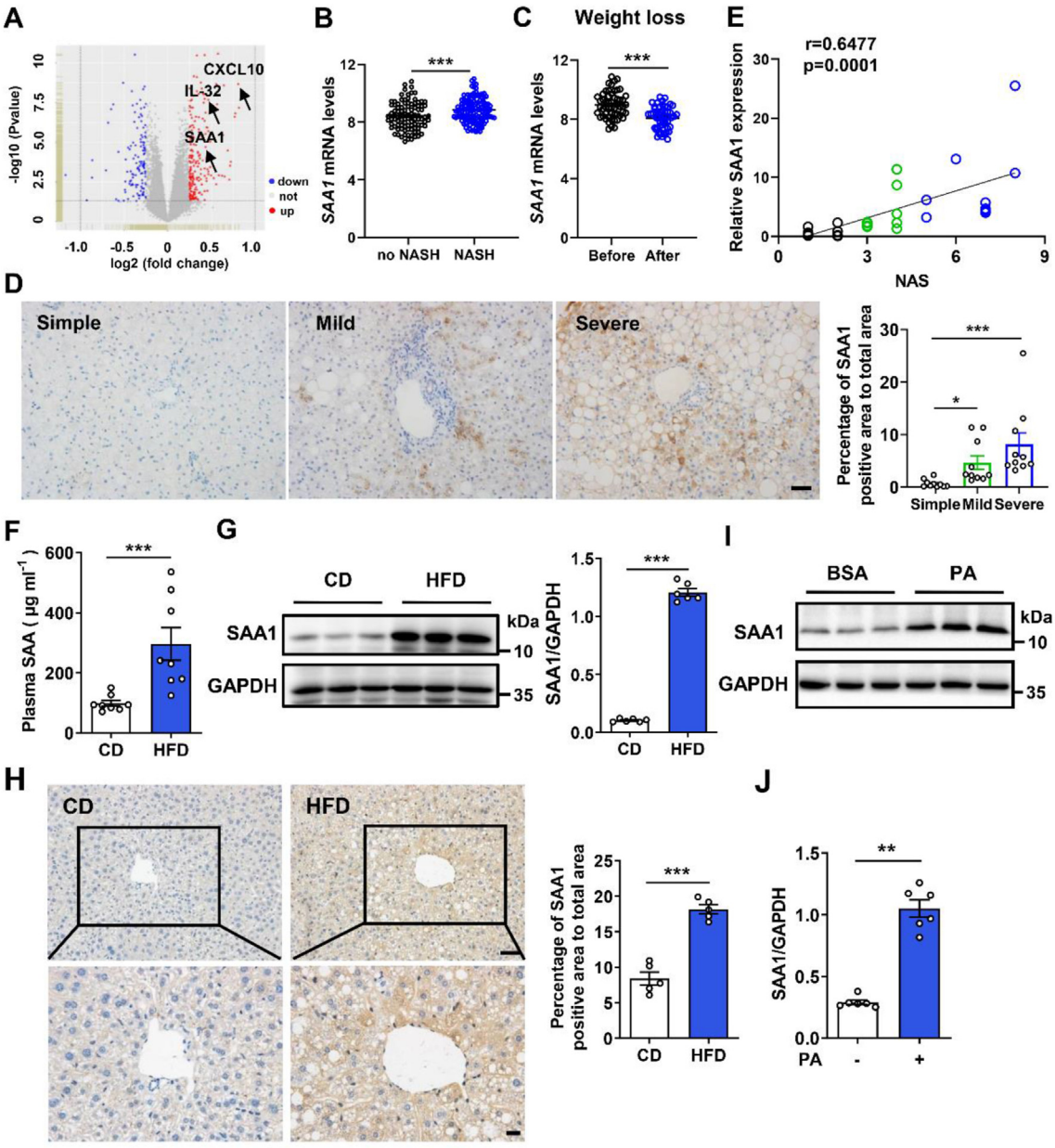

Figure 1: SAA1 expression is upregulated in fatty liver from NAFLD patients and obese mice. (**A**) Volcano plots indicating differentially expressed genes (DEGs; red, upregulated genes; blue, downregulated genes) in NASH compared with no NASH human liver biopsies (GSE83452). (**B**) SAA1 mRNA level in no NASH (n = 98) and NASH (n = 126) human liver biopsies. (**C**) SAA1 mRNA level in the liver of human after weight loss in paired obese subjects (n = 54). (**D**) IHC staining (left) and quantifications (right) of SAA1 in simple, mild, and severe NAFLD human liver biopsies (n = 10 per group). Scale bars, 50 μm. (**E**) Correlation analysis of SAA1 protein level with NAS score in human liver samples (n = 30). (**F**) Male C57BL/6J mice were fed a CD or HFD for 16 weeks. Plasma concentrations of SAA in CD- and HFD-fed mice (n = 8). (**G**) Representative western blot images (left) and quantifications (right) of SAA1 expressions in liver tissues of CD- and HFD-fed mice (n = 6). (**H**) IHC staining (left) and quantifications (right) of SAA1 in liver tissues of CD- and HFD-fed mice (n = 5). Scale bars, 50 μm (top) and 20 μm (bottom). (**I, J**) Representative western blot images (I) and quantifications (J) of SAA1 expression in primary mouse hepatocytes that were treated with PA (0.25 mM) or BSA for 4 h (n = 6). All data are expressed as means ± SEMs. *P < 0.05, **P < 0.01, ***P < 0.001. (For interpretation of the references to color in this figure legend, the reader is referred to the Web version of this article.)

3. RESULTS

3.1. Increased level of SAA1 is associated with NAFLD

We analyzed human liver transcriptome profiles from a published transcriptome dataset composed of 98 non-NASH and 126 NASH liver samples (GSE83452) [27]. Expressional levels of several well-known proinflammatory mediators, such as C-X-C motif chemokine ligand 10 (*CXCL10*) [28] and *IL-32* [29], were increased in NASH liver samples (Figure 1A and Supplementary Fig. 1A). Of note, we found that the expression of SAA1, the major form of SAA that is an indicator of inflammation, was also significantly higher in NASH livers than in NASH-free livers (Figure 1B). The weight loss by dietary intervention or gastric bypass surgery decreased the hepatic expression of SAA1 in the paired samples (Figure 1C). This finding prompted us to investigate the role of SAA1 in NAFLD. We collected 30 liver tissues from patients with NAFLD to perform IHC staining. We found the increased SAA1

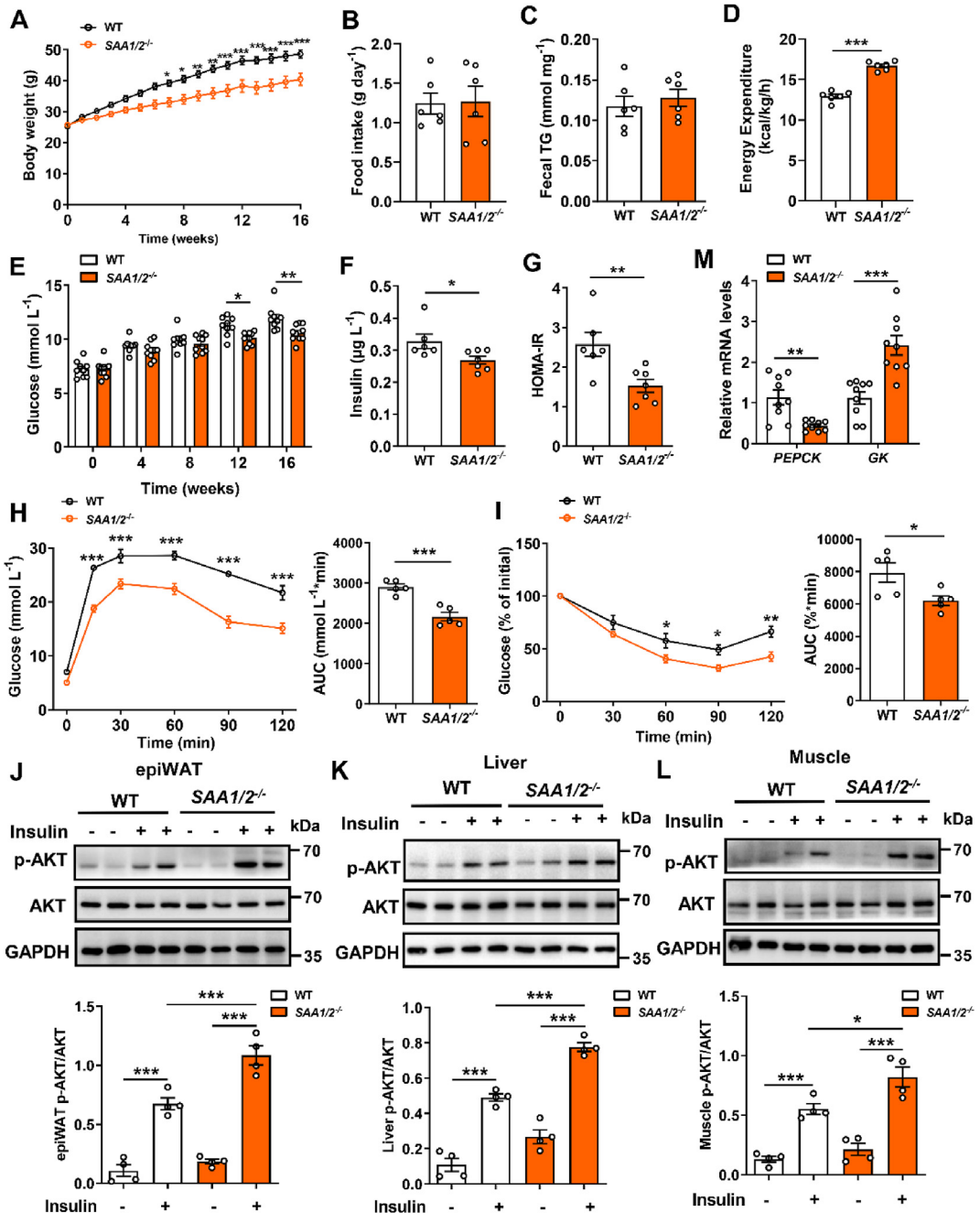

Figure 2: SAA1/2 deficiency protects HFD-induced glucose disorders and insulin resistance. Male WT and *SAA1/2*$^{-/-}$ mice were fed a HFD for 16 weeks. (**A**) Body weight during 16 weeks HFD feeding in WT (n = 9) and *SAA1/2*$^{-/-}$ mice (n = 10). (**B**) Averaged daily food intake in HFD-fed WT and *SAA1/2*$^{-/-}$ mice (n = 6). (**C**) Fecal TG content from WT and *SAA1/2*$^{-/-}$ mice fed a HFD for 3 weeks (n = 6). (**D**) Energy expenditure in HFD-fed WT and *SAA1/2*$^{-/-}$ mice (n = 6). (**E**) Fasting blood glucose in WT (n = 9) and *SAA1/2*$^{-/-}$ (n = 10) mice. (**F, G**) Fasting blood insulin concentrations (F) and HOMA-IR (G) in WT (n = 6) and *SAA1/2*$^{-/-}$ (n = 7) mice. HOMA-IR index was calculated according to the following formula: (fasting insulin × fasting glucose)/22.5. (**H, I**) GTT (H) and ITT (I) in WT and *SAA1/2*$^{-/-}$ mice (n = 5). (**J-L**) Representative western blot images (top) and quantifications (bottom) of AKT phosphorylation in epiWAT (J), liver (K), and skeletal muscle (L) from WT and *SAA1/2*$^{-/-}$ mice stimulated by insulin (n = 4). (**M**) mRNA levels of *PEPCK* and *GK* of livers from WT and *SAA1/2*$^{-/-}$ mice (n = 9). All data are expressed as means ± SEMs. *P < 0.05, **P < 0.01, ***P < 0.001.

expression in mild and severe NAFLD livers compared to that in simple NAFLD controls (Figure 1D). Moreover, hepatic SAA1 level was positively correlated with NAFLD activity score (NAS) (Figure 1E) and ALT, but not with AST or TG (Supplementary Figs. 1B—D) in human subjects.

We also examined SAA1 expression profiles in HFD-induced mouse steatohepatitis model. Compared to the mice fed a CD, the plasma level of SAA was significantly increased in the mice after HFD feeding for 16 weeks (Figure 1F). The SAA1 expression was also markedly increased in the liver, but not in the epididymal white adipose tissue (epiWAT), muscle or heart, of HFD mice (Figure 1G and Supplementary Figs. 1E—G). IHC staining confirmed the increased SAA1 expression in hepatic steatosis tissues (Figure 1H). Consistently, SAA1 levels in both liver and plasma were increased in the

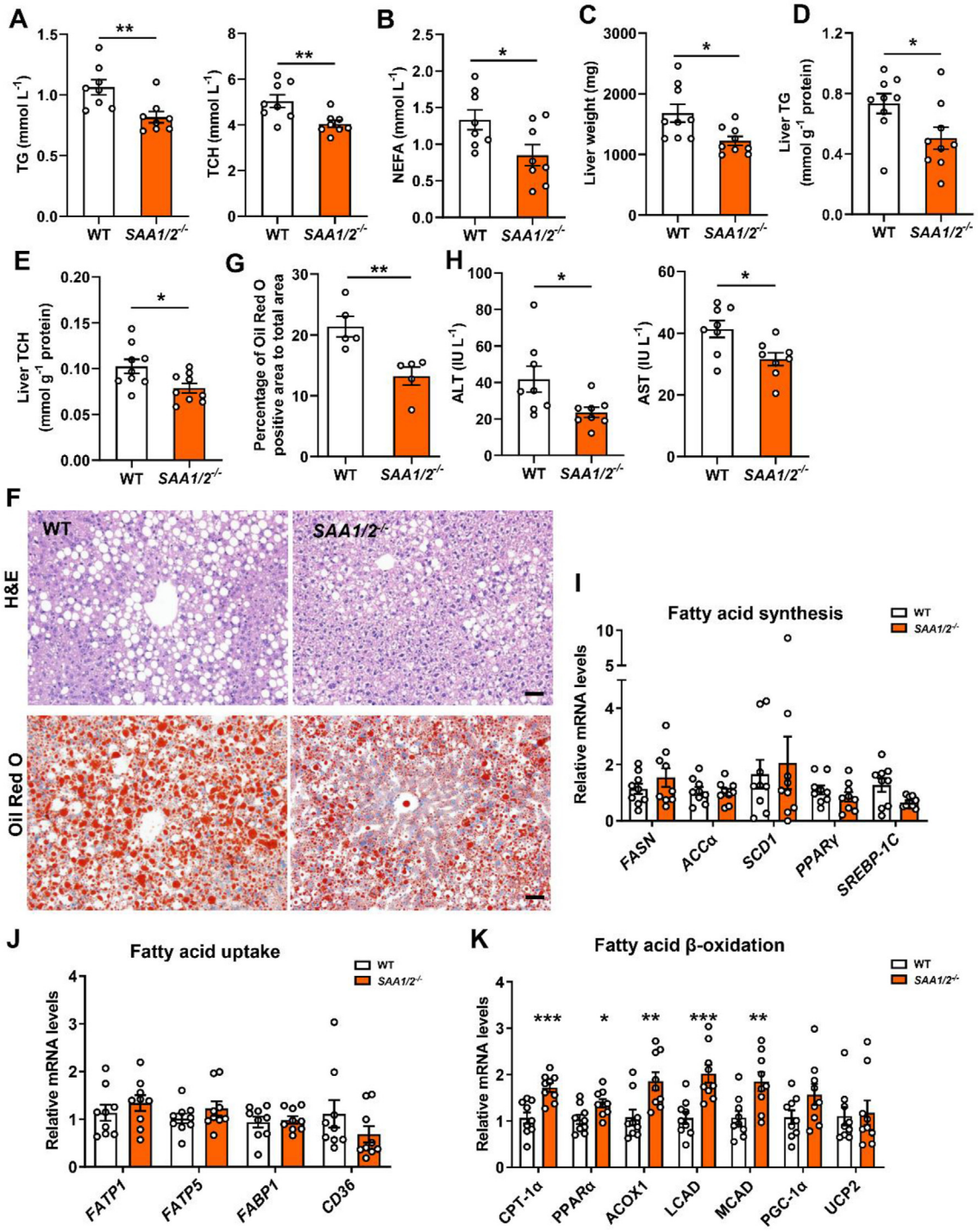

Figure 3: SAA1/2 deficiency protects against hepatic steatosis. Male WT and *SAA1/2*$^{-/-}$ mice were fed a HFD for 16 weeks. (**A**) TG (left) and TCH (right) levels in the plasma of HFD-fed WT and *SAA1/2*$^{-/-}$ mice (n = 8). (**B**) NEFA levels in the plasma of HFD-fed WT and *SAA1/2*$^{-/-}$ mice (n = 8). (**C**) The liver weights of *SAA1/2*$^{-/-}$ mice and controls at 16 weeks post-HFD administration (n = 9). (**D, E**) Liver TG (D) and TCH (E) levels in WT and *SAA1/2*$^{-/-}$ mice (n = 9). (**F**) Representative images showing H&E staining (upper) and Oil Red O staining (bottom) of liver sections from WT and *SAA1/2*$^{-/-}$ mice that were fed a HFD for 16 weeks. Scale bar, 50 μm. (**G**) Quantifications of lipid droplet area in Oil Red O staining of representative liver sections (n = 5). (**H**) Plasma levels of ALT (left) and AST (right) in WT and *SAA1/2*$^{-/-}$ mice (n = 8). (**I**–**K**) mRNA levels of fatty acid synthesis (I), fatty acid uptake (J), and fatty acid β-oxidation (K) genes in the livers from WT and *SAA1/2*$^{-/-}$ mice (n = 9). All data are expressed as means ± SEMs. *P < 0.05, **P < 0.01, ***P < 0.001. (For interpretation of the references to color in this figure legend, the reader is referred to the Web version of this article.)

mice fed a WD for 8 weeks (Supplementary Figs. 1H and I). *In vitro* experiments revealed that palmitic acid (PA) but not bovine albumin (BSA) could induce the upregulation of SAA1 in cultured mouse primary hepatocytes (Figure 1I,J). These results suggest that increased levels of SAA1 in circulation and liver may be associated with NAFLD.

3.2. SAA1/2 deficiency attenuates HFD-induced obesity and insulin resistance in mice

To investigate the possible causal link between SAA1 and NAFLD, we generated *SAA1/2*$^{-/-}$mice with no discernible defects at weaning by CRISPR/Cas9 system (Supplementary Figs. 2A and B). Deletion of the *SAA1/2* gene significantly decreased plasma level of SAA in the LPS-administered mice (Supplementary Fig. 2C). No SAA1 protein could be detected in the *SAA1/2*$^{-/-}$ mouse livers (Supplementary Fig. 2D). Deficiency in SAA1/2 did not alter murine body weight, food intake, and blood glucose metabolism in the CD-fed mice (Supplementary Figs. 3A—F). However, it attenuated HFD-induced gain of body weight (Figure 2A). The effect of SAA1/2 deletion on body weight gain was independent of food consumption (Figure 2B) and absorption of dietary lipids (Figure 2C). *SAA1/2*$^{-/-}$ mice showed more energy expenditure than WT mice (Figure 2D), revealing an improvement of metabolic dysregulation in *SAA1/2*$^{-/-}$ mice. Moreover, SAA1/2 deficiency attenuated the disorder of glucose metabolism in mice (Figure 2E—I). Knockout of SAA1/2 promoted insulin-induced phosphorylation of AKT in epiWAT, liver, and skeletal muscle in HFD mice (Figure 2J-L). In line with the increased activation of insulin signaling, the downregulation of gluconeogenesis enzymes *PEPCK* and the upregulation of *Glucokinase* (*GK*) were found in the liver of *SAA1/2*$^{-/-}$ HFD mice (Figure 2M). These results indicate that the deficiency of SAA1/2 ameliorates the HFD-induced insulin resistance in mice.

3.3. SAA1/2 deficiency attenuates HFD-induced hepatic steatosis

We then examined the effects of SAA1/2 deficiency on hepatic steatosis. Deletion of the *SAA1/2* gene alone did not influence lipid metabolism and liver function in mice (Supplementary Figs. 3G—J). It attenuated HFD-induced hyperlipidemia including high plasma levels of TG, TCH, and NEFA in mice (Figure 3A,B). The liver weight and liver TG and TCH were also significantly reduced in HFD-fed *SAA1/2*$^{-/-}$ mice (Figure 3C—E). In agreement with it, fewer lipid droplets were found in the HFD-challenged *SAA1/2*$^{-/-}$ livers, as visualized by H&E staining and Oil Red O staining (Figure 3F,G). Consistently, HFD-fed *SAA1/2*$^{-/-}$ mice exhibited ameliorated liver dysfunction as measurements of plasma ALT and AST concentrations (Figure 3H).

SAA1/2 deficiency led to an upregulation of fatty acid β-oxidation-related genes, including carnitine palmitoyl transferase 1α (*CPT-1α*), peroxisome proliferator activated receptor α (*PPARα*), acyl-CoA oxidase 1 (*ACOX1*), long-chain acyl-CoA dehydrogenase (*LCAD*), and medium-chain acyl-CoA dehydrogenase (*MCAD*), in HFD livers (Figure 3K). However, no dramatic changes in the expression of the genes related to fatty acid synthesis (Figure 3I) and fatty acid uptake (Figure 3J) were found. These data reveal that SAA1/2 deficiency promotes lipid catabolism in murine liver.

We also used recombinant AAV8-shRNA-*SAA1/2* to specifically knockdown hepatic SAA1/2 (Supplementary Fig. 4A) to confirm the pathogenetic role of SAA1/2 in hepatic steatosis. The suppressed SAA1/2 maintained for 16 weeks after the administration by AAV8-shRNA-*SAA1/2* (Supplementary Fig. 4B). Knockdown of SAA1/2 attenuated HFD-induced gain of body weight (Supplementary Fig. 4C) and insulin resistance (Supplementary Figs. 4D—H). As expected, it also inhibited HFD-induced lipid accumulation in murine liver (Supplementary Fig. 4I-N).

Effect of SAA1/2 deficiency on hepatic lipid accumulation was further validated by *in vitro* experiments. Oil Red O staining displayed that SAA1/2 deficiency ameliorated lipid accumulation in cultured primary mouse hepatocytes treated by PA (Supplementary Figs. 5A and B). The intracellular level of TG was also decreased in *SAA1/2*$^{-/-}$ hepatocytes compared to WT cells (Supplementary Fig. 5C). Conversely, treatment with recombinant mouse SAA1 promoted lipid accumulation in cultured hepatocytes (Supplementary Figs. 5D—F). Taken together, these findings clearly demonstrate that SAA1 may promote overnutrition-induced NAFLD.

3.4. Loss of SAA1/2 mitigates HFD-induced hepatic inflammatory response

To understand the mechanism underlying SAA1 promoting NAFLD, we further investigated the role of SAA1 in obesity-induced chronic inflammation. IHC staining showed that there was an accumulation of F4/80^{+} macrophages in HFD-fed murine livers which was mitigated by SAA1/2 deficiency (Figure 4A). Measurements of mRNA levels of macrophages marker, *CD68* and *F4/80*, confirmed this observation (Figure 4B). Furthermore, HFD-fed *SAA1/2*$^{-/-}$ mice showed reduced levels of hepatic pro-inflammatory cytokines, including TNF-α, IL-1β, IL-6 and chemokine CCL2 compared to WT controls (Figure 4C,D). This was corroborated by measurements of plasma levels of CRP (Figure 4E). In addition, the deficiency of SAA1/2 suppressed MAPK signaling by blocking phosphorylation of JNK and p38 and canonical NF-κB signaling by blocking phosphorylation of IKK and p65 in the HFD liver (Figure 4F,G). Collectively, these data reveal that SAA1/2 deficiency inhibits HFD-induced inflammation in mice.

To further define the role of hepatic SAA1 in HFD-induced inflammation, we isolated primary mouse hepatocytes to observe the PA-induced inflammatory response. Expression of pro-inflammatory mediators IL-6 and CCL2 in the hepatocytes was suppressed by SAA1/2 knockout at transcriptional (Figure 4H) and translational (Figure 4I) levels *in vitro*. When recombinant mouse SAA1 was directly administered into the cultured primary mouse hepatocytes, the levels of IL-6 and CCL2 were increased both dose- (Figure 4J,K) and time-dependently (Supplementary Figs. 6A and B). Treatment with SAA1 directly activated MAPKs and NF-κB signaling pathways in a concentration-dependent manner (Figure 4L and Supplementary Figs. 6C—F). Activation of JNK, p38, IKK, and p65 by SAA1 treatment was also transient (Supplementary Figs. 6G—K). The SAA1-induced production of IL-6 and CCL2 was entirely abrogated by treatment of cells with the selective NF-κB inhibitor Bay11-7082 (Figure 4M and N). *In vivo* experiment showed that specific knockdown of hepatic SAA1/2 by using AAV8-shRNA-*SAA1/2* could inhibit the F4/80 positive macrophages infiltration and *IL-1β*, *IL-6*, and *CCL2* production in the HFD liver (Supplementary Figs. 7A and B). Thus, SAA1 may directly induce inflammatory response in hepatocytes by activating NF-κB signaling.

3.5. TLR4 is necessary for SAA1-related hepatic steatosis and inflammation

NF-κB is a downstream signaling linked by TLR4. To investigate whether TLR4 was implicated in SAA1-associated hepatic steatosis, we deleted *TLR4* to duplicate HFD-induced hepatic steatosis. The AAV8-SAA1-transfected mice (Figure 5A,B) showed dramatical alleviation in gain of body weight and insulin resistance by TLR4 deletion (Figure 5C—F). The AAV8-SAA1-aggravated hepatic lipid accumulation and liver injury were significantly attenuated in HFD *TLR4*$^{-/-}$ mice compared to that in HFD WT mice (Figure 5G-L, Supplementary Figs. 8A and B).

Consistently, infiltration of F4/80 positive macrophages and overproduction of pro-inflammatory mediators *IL-1β*, *IL-6* and *CCL2* by SAA1 were obviously inhibited in the *TLR4*$^{-/-}$ liver (Figure 5J, M, N). Observations from *in vitro* investigations confirmed these results (Figure 6A—C and Supplementary Fig. 8C), suggesting that TLR4 may be necessity for SAA1-associated hepatic steatosis and inflammation.

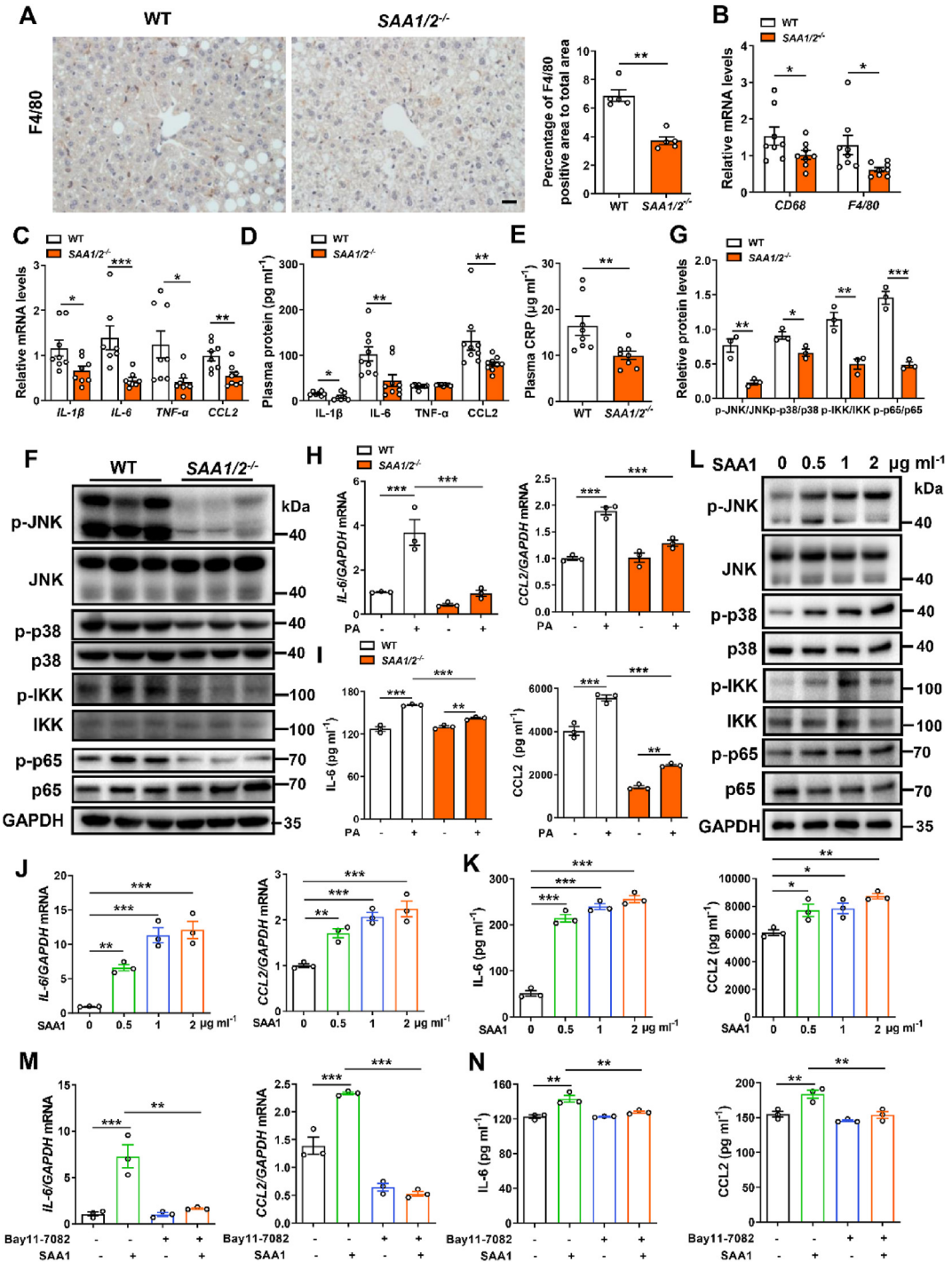

Figure 4: SAA1/2 promotes hepatic inflammatory response. Male WT and *SAA1/2*$^{-/-}$ mice were fed a HFD for 16 weeks. (**A**) Representative IHC images (left) and quantifications (right) of F4/80 positive macrophages in the livers of WT and *SAA1/2*$^{-/-}$ mice (n = 5). Scale bar, 20 μm. (**B**) mRNA levels of the markers of macrophages indicated in the livers of WT and *SAA1/2*$^{-/-}$ mice (n = 8). (**C**) mRNA levels of inflammatory cytokines *IL-1β*, *IL-6*, *TNF-α* and chemokine *CCL2* in the liver of WT and *SAA1/2*$^{-/-}$ mice (n = 7–8). (**D**) Plasma concentrations of IL-1β, IL-6, TNF-α and CCL2 in HFD-fed WT and *SAA1/2*$^{-/-}$ mice. IL-1β, n = 7. IL-6, TNF-α and CCL2, n = 9. (**E**) Plasma concentrations of CRP in HFD-fed WT and *SAA1/2*$^{-/-}$ mice (n = 8). (**F, G**) Representative western blot images (F) and quantifications (G) of the expression levels of key proteins in MAPKs and NF-κB signaling in the liver of HFD-fed WT and *SAA1/2*$^{-/-}$ mice (n = 3). (**H, I**) Hepatocytes isolated from CD-fed WT and *SAA1/2*$^{-/-}$ mice were treated with PA (0.25 mM) for 4 h mRNA levels of inflammatory mediators (*IL-6* and *CCL2*) were assessed by qRT-PCR (n = 3) (H). IL-6 and CCL2 levels in hepatocytes culture media were determined using ELISA (n = 3) (I). (**J, K**) Hepatocytes isolated from CD-fed WT mice were treated with indicated concentrations of recombinant mouse SAA1 for 4 h mRNA levels (J) and culture media (K) of IL-6 and CCL2 were determined (n = 3). (**L**) Representative western blot images of the expression levels of key proteins in MAPKs and NF-κB signaling in hepatocytes that were treated with indicated concentrations of SAA1 for 30 min. (**M, N**) Hepatocytes isolated from CD-fed WT mice were treated with or without PA (0.25 mM) or NF-κB pathway inhibitor Bay-117,082 (10 μM) for 4 h mRNA levels (M) and culture media (N) of IL-6 and CCL2 were determined (n = 3). All data are expressed as means ± SEMs. *P < 0.05, **P < 0.01, ***P < 0.001.

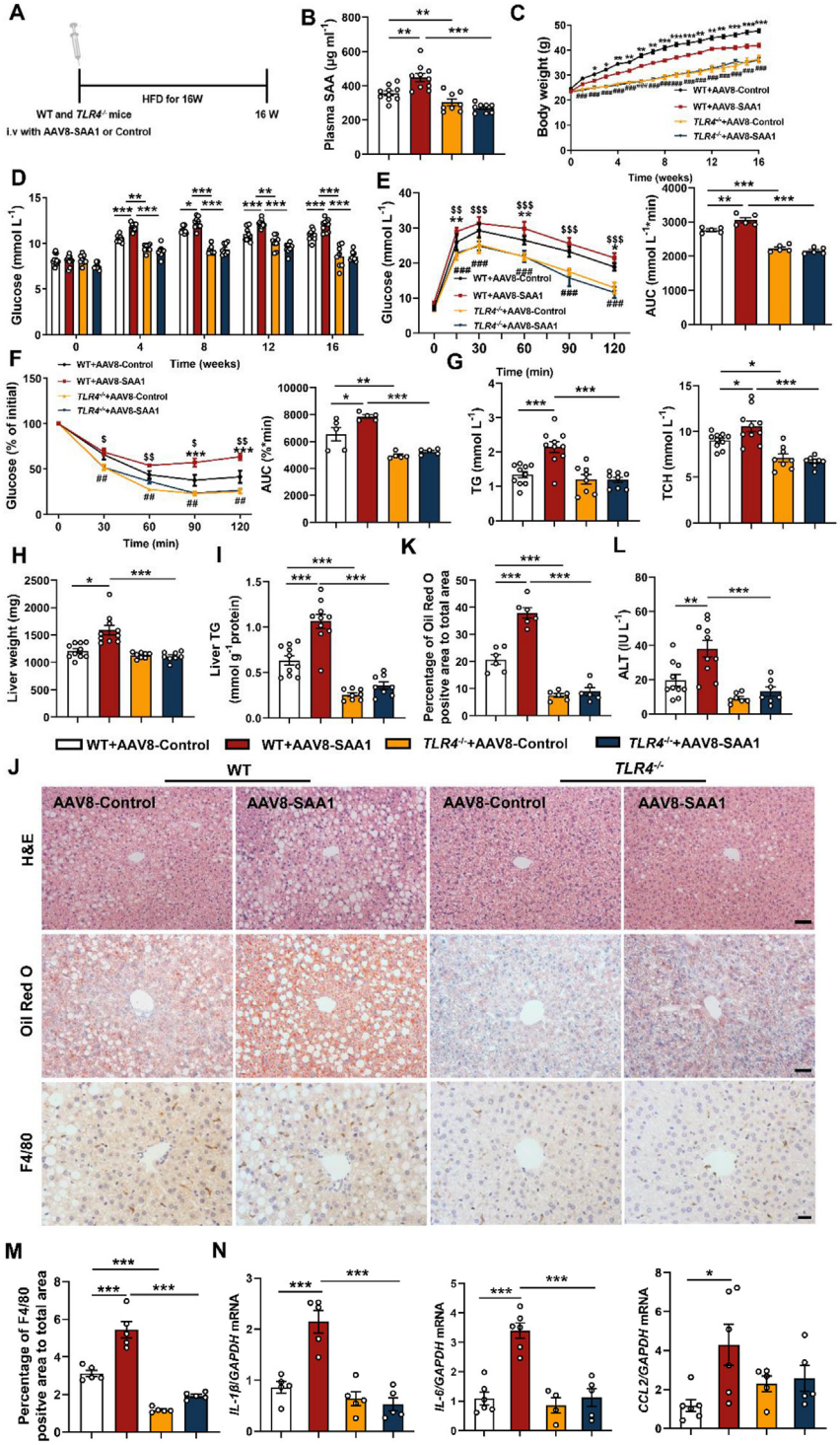

Figure 5: SAA1 promotes hepatic lipid accumulation and inflammation in an TLR4-dependent manner. Male *TLR4*$^{-/-}$ and control mice were tail vein injected with AAV8-con or AAV8-SAA1 and then fed a HFD for 16 weeks. (**A**) Schematic of the experimental design of AAV8 treatment in *TLR4*$^{-/-}$ and control mice model. (**B**) Plasma concentrations of SAA from *TLR4*$^{-/-}$ (n = 8) and control mice (n = 10) treated with AAV8-con or AAV8-SAA1. (**C**) Body weight during 16 weeks HFD feeding in *TLR4*$^{-/-}$ (n = 8) and control mice (n = 10). (**D**) Fasting blood glucose in *TLR4*$^{-/-}$ (n = 8) and control mice (n = 10). (**E, F**) GTT (E) and ITT (F) in *TLR4*$^{-/-}$ and control mice (n = 5). (**G**) TG (left) and TCH (right) levels in the plasma of HFD-fed *TLR4*$^{-/-}$ (n = 8) and control mice (n = 10). (**H**) The liver weights of *TLR4*$^{-/-}$ (n = 8) and control mice (n = 10). (**I**) Liver TG levels were determined in *TLR4*$^{-/-}$ (n = 8) and control mice (n = 10). (**J**) Representative images showing H&E staining (upper), Oil Red O staining (middle) and F4/80 positive macrophages staining (bottom) of liver sections of *TLR4*$^{-/-}$ and control mice. H&E staining and Oil Red O staining, scale bar, 50 μm. F4/80 positive cells staining, scale bar, 20 μm. (**K**) Quantifications of lipid droplet area in Oil Red O staining of representative liver sections (n = 6). (**L**) Plasma levels of ALT in *TLR4*$^{-/-}$ (n = 7) and control mice (n = 10). (**M**) Quantifications of F4/80 positive area of representative liver sections (n = 5). (**N**) mRNA levels of inflammatory mediators in the liver of *TLR4*$^{-/-}$ and control mice (n = 4–6). All data are expressed as means ± SEMs. *, WT + AAV8-Control VS WT + AAV8-SAA1. $, WT + AAV8-Control VS *TLR4*$^{-/-}$ + AAV8-Control. #, WT + AAV8-SAA1 VS *TLR4*$^{-/-}$ + AAV8-SAA1. *P < 0.05, **P < 0.01, ***P < 0.001. (For interpretation of the references to color in this figure legend, the reader is referred to the Web version of this article.)

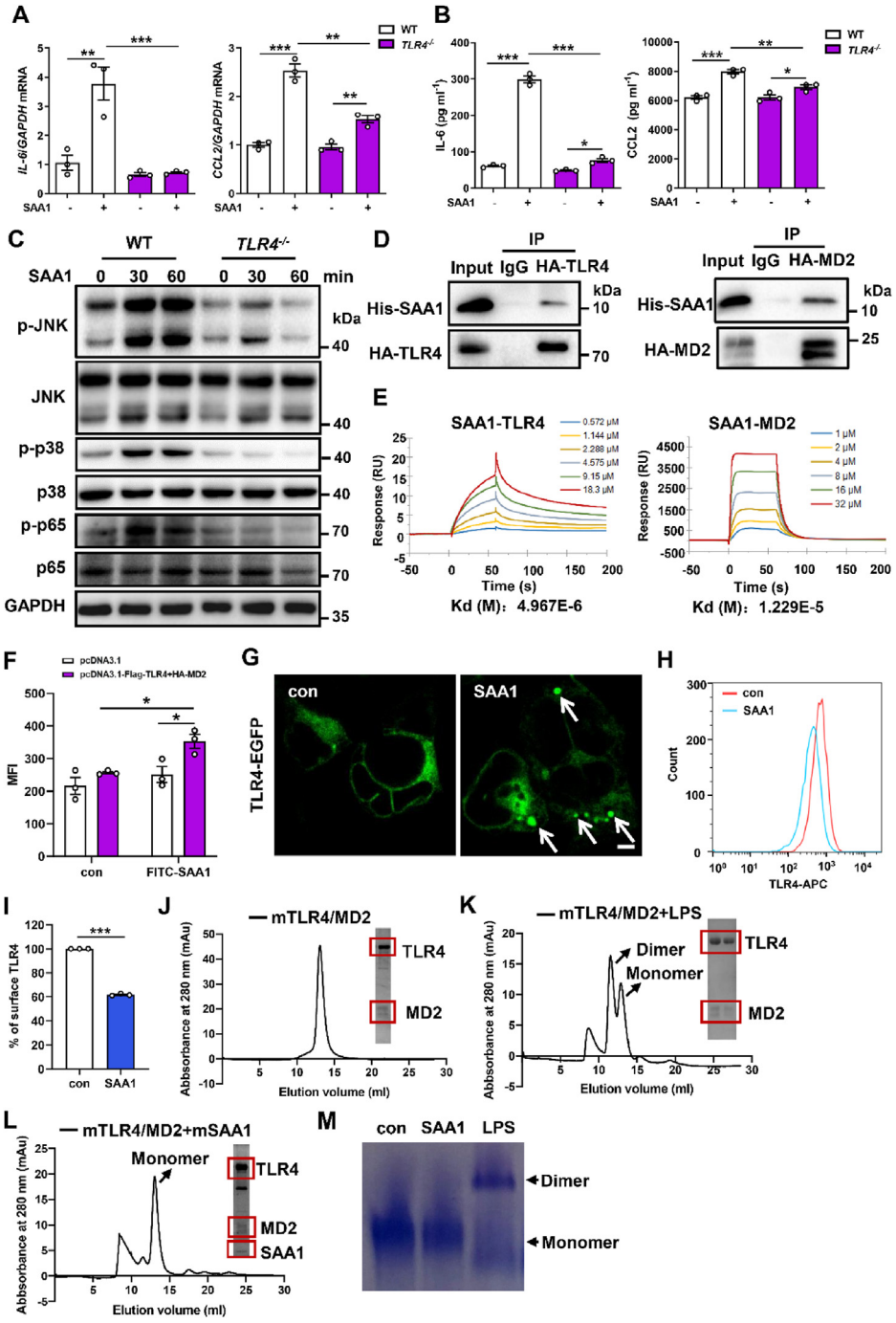

Figure 6: SAA1/2 directly binds to TLR4 and its accessory protein MD2, mediating TLR4 activities. Hepatocytes isolated from CD-fed male *TLR4*$^{-/-}$ and control mice were treated with SAA1 (2 μg ml^{-1}) for 4 h. (**A**) mRNA levels of *IL-6* and *CCL2* were assessed by qRT-PCR (n = 3). (**B**) IL-6 and CCL2 levels in hepatocytes culture media were determined using ELISA (n = 3). (**C**) Representative western blot images of the expression levels of key proteins in MAPKs and NF-κB signaling in hepatocytes from *TLR4*$^{-/-}$ and control mice that were treated with SAA1 (2 μg ml^{-1}) for indicated time. (**D**) Co-IP assays were performed in HEK293 cells co-transfected with HA-tagged TLR4 (left) or HA-tagged MD2 (right) plasmids to examine the SAA1-TLR4 or MD2 interaction. (**E**) Representative graphs from surface plasmon resonance spectroscopy analysis showing the binding of recombinant mouse SAA1 with recombinant mouse TLR4 (left) or MD2 (right). (**F**) HEK293 cells transfected with Flag-TLR4 and HA-MD2 plasmids followed by incubation with FITC-labeled SAA1. Cell-associated fluorescence was estimated using a fluorescence plate reader. (**G**) Confocal microscopy results of the internalization of TLR4-EGFP in TLR4-MD2-transfected HEK293 cells treated with SAA1 (2 μg ml^{-1}). Scale bar, 5 μm. (**H**, **I**) Hepatocytes treated with SAA1 (2 μg ml^{-1}) for 120 min and TLR4 endocytosis was determined by flow cytometry (n = 3). (**J-L**) Dimerization of mouse TLR4-MD2 complex mediated by ligands was examined by size-exclusion chromatography (Superdex 200) and SDS-PAGE with Coomassie staining. The monomeric mouse TLR4-MD2 complexes (J), incubation of TLR4-MD2 complex with LPS (K) and incubation of TLR4-MD2 complex with mouse recombinant SAA1 were determined (L). (**M**) After the reaction between mouse recombinant SAA1 or LPS and mouse TLR4-MD2 under the indicated conditions, the samples loaded at gradient Native PAGE (4–15%) were visualized with Coomassie staining. Representative results from three independent experiments are shown. All data are expressed as means ± SEMs. *P < 0.05, **P < 0.01, ***P < 0.001.

3.6. SAA1 directly binds to TLR4 and the accessory protein MD2 triggering TLR4 internalization

SAAs is supposed as an endogenous TLR4 agonist [30]. We examined the direct interaction between SAA1 and TLR4 by performing co-IP assays. Interestingly, when HA-tagged TLR4 or its accessory protein MD2 plasmids were transfected into HEK293 cells, co-IP with HA antibody showed that both HA-TLR4 and HA-MD2 directly interacted with purified SAA1 protein (Figure 6D). We then used SPR to evaluate direct interaction between SAA1 and TLR4 or MD2 in cell-free system. It was shown that SAA1 interacted directly with recombinant mouse TLR4 with a KD of 496.7 nM and recombinant mouse MD2 with a KD of 122.9 nM (Figure 6E), revealing that SAA1 may directly associated with TLR4 and MD2 protein and initiate TLR4-MD2 inflammatory signaling. The ligand-induced receptor internalization is a key event in the activation of the TLR4 pathway [25]. We found that FITC-labeled SAA1 specifically interacted with TLR4-MD2 in the transfected HEK293 cells (Figure 6F). Confocal microscopy observation showed that SAA1 triggered TLR4 internalization into the cell (Figure 6G). We also monitored the translocation of TLR4 by cell-surface staining of TLR4 and flow cytometry. Treatment of hepatocytes with SAA1 resulted in approximately 40% of TLR4 leaving from the cell surface within 120 min (Figure 6H,I). Collectively, these results provide evidence that TLR4 may be an authentic and specific receptor for SAA1 in hepatocytes.

The dimerization of TLR4-MD2 would be required for internalization of TLR4-MD2 to initiate TLR4 pathway activation [31]. Size-exclusion chromatography test showed that the monomeric mouse TLR4-MD2 complex was eluted around the 14 ml fraction (~90 kDa) (Figure 6J). While incubation with LPS, a typic ligand of TLR4, a significantly forward shifted peak was eluted around at the 12 ml fraction (~180 kDa), which was identified as dimerized TLR4-MD2 complex (Figure 6K). Surprisingly, the TLR4-MD2 complex incubated with SAA1 was still eluted at the 14 ml fraction, indicating that TLR4-MD2 complex remained as a monomeric complex in the presence of SAA1 (Figure 6L). Consistent observation was also received by a native PAGE (Figure 6M). These results suggest that SAA1 may not directly initiate dimerization of TLR4-MD2 to trigger TLR4 internalization in cells.

3.7. SAA1/TLR4/NF-κB/SAA1 circuit drives inflammatory response in hepatocytes contributing to hepatic steatosis progression

It is noted that both SAA1 and TLR4 are expressed in hepatocytes and participate cellular inflammatory response and lipid accumulation. To further identify the role of SAA1 in the cellular inflammatory response, we determined the influence of exogenous SAA1 on its expression in cells. We found that SAA1 expression was significantly enhanced upon administration of hepatocytes by recombinant mouse SAA1 (Supplementary Figs. 9A and B). It was completely blocked by TLR4 deletion (Supplementary Fig. 9C). Selective suppression of NF-κB signaling by using inhibitor Bay11-7082 had a similar effect (Supplementary Fig. 9D). These results suggest that SAA1 may stimulate hepatocytes to produce itself by a TLR4-NF-κB signaling-mediated autocrine manner.

We finally verified the potential therapeutic effect of targeting SAA1 on murine steatohepatitis. The 6 weeks of HFD-feeding mice were administered by an AAV8-shRNA-*SAA1/2* or AAV8-shRNA-sc and were continuously fed by a HFD for another 10 weeks (Figure 7A). Knockdown of hepatic SAA1 decreased plasma level of SAA1 and body weight (Figure 7B,C). It improved HFD-induced insulin resistance (Figure 7D—F). Knockdown of hepatic SAA1 did inhibit F4/80 positive macrophages infiltration and pro-inflammatory mediators' production in livers (Figure 7G—I). Importantly, murine steatohepatitis was attenuated by knockdown of hepatic SAA1 (Figure 7J-N). Consistently, relative to mice injected by the AAV8-shRNA-sc, the AAV8-shRNA-*SAA1/2*-administrated mice had a considerable reduction in ALT (Figure 7O) and upregulation of fatty acid β-oxidation-related genes (Supplementary Figs. 10A—C). As such, these findings provide support for the notion that SAA1 may act as both a trigger and effector for hepatic inflammation contributing to the progression of NAFLD.

4. DISCUSSION

Inflammation is considered an adaptive response to tissue injury or infection to coordinate cellular defense system and tissue repair. Overnutrition-induced persistent hepatic inflammation exacerbates sublethal lipotoxic injury and prevents wound healing response in liver that contributes to the development of NASH and liver fibrosis. Therefore, triggering chronic liver inflammation is specially paid attention in transition from NAFLD to NASH [7,32,33]. In the present study, we found that SAA1, serves as an acute phase protein, inflammatory cytokine, and chemokine, triggered hepatic inflammation and promoted progression of NAFLD. SAA1 could directly bind with TLR4 and MD2 inducing TLR4 internalization and activation of NF-κB signaling, which in turn led to production of SAA1 in hepatocytes. Our results highlight the novel role of SAA1 in liver inflammation and provide a potential target for antagonizing progression of NAFLD.

It is reported that SAA1 induces lipolysis of fat through an extracellular signal regulated kinase (ERK)-dependent pathway that leads to elevation of circulating NEFA [34]. Consistent with this finding, our results showed that SAA1 inhibited fatty acid β-oxidation in liver without affecting fatty acid synthesis and uptake, thereby exacerbating over-nutrition-induced obesity and inhibiting energy expenditure. The insulin resistance-promoting effect of SAA1 was mediated by suppression of AKT signaling. However, the increased AKT phosphorylation was accompanied with the unaltered sterol regulatory element binding transcription factor-1C (SREBP-1C) expression in SAA1-deficient murine liver. Consistent observations are also reported in other inflammation-driven NAFLD models, in which the inflammatory mediators have impact to enhance lipid synthesis [35,36]. The increase in NEFA and suppression of its metabolism in hepatocytes induced by SAA1 may promote the development of NASH.

Unlike most inflammatory cytokines, SAA has pleotropic effects *in vitro* with both pro-inflammatory and anti-inflammatory characteristics. Its proinflammatory ability resides in its role in mediating innate and adaptive immune system by inducing the production of various cytokines and chemokines and activating the inflammasome pathway [19,37]. On the other hand, it promotes inflammation resolution by shifting macrophages toward the M2 phenotype and antagonizes LPS-induced inflammation and tissue injury [38,39]. Administration of SAA fails to increase the plasma levels of pro-inflammatory cytokines [40]. These contradictory observations may reflect the flexible features of SAA in the acute-phase response, in which hepatic SAA is released out by stimulation of inflammatory cytokines such as IL-6, TNF-α and IL-1β. The SAA-related rapid parallel mobilization of myeloid-derived suppressor cells mediates feedback inflammation inhibition and resolution [11]. Local microenvironment may also set the tone of SAA1 in disease pathogenesis. The systemic, chronic, and low-grade inflammation induced by obesity causes persistent elevation of SAA in the body. Moreover, we demonstrate that SAA1 could directly activate TLR4-NF-κB signaling pathway for inflammatory response in liver cells. This intrahepatic inflammation triggered by SAA1 and other possible factors results in further hepatocyte damage and progression of NAFLD. Thus, SAA1 may act as a trigger for NAFLD progression by inflammation-prone features secondary to the reduced energy expenditure.

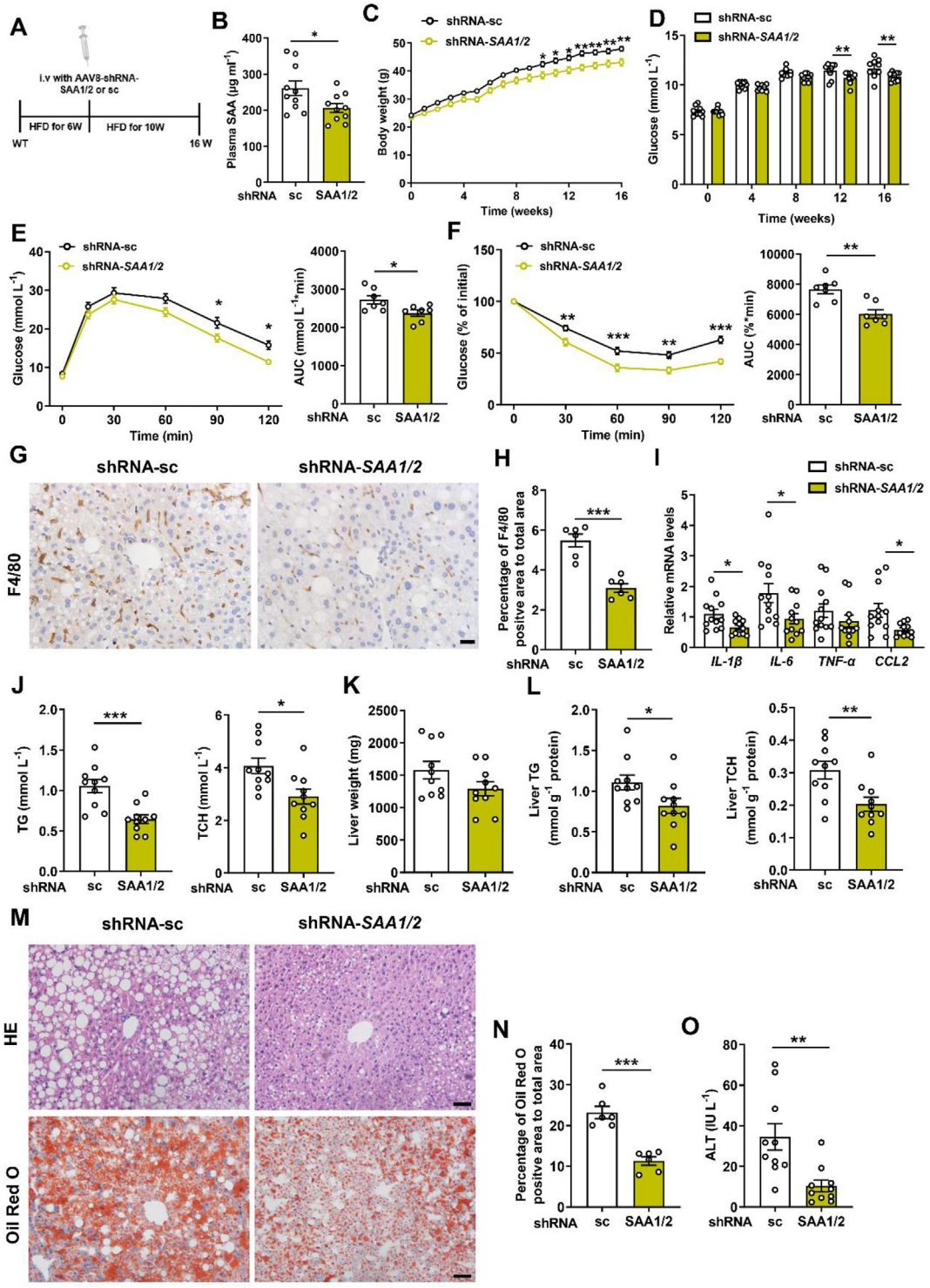

Figure 7: Effects of knockdown of SAA1/2 on steatohepatitis and metabolic syndrome in HFD mice. Male C57BL/6J mice were fed a HFD for 6 weeks, and their tail vein was then injected with AAV8-shRNA-sc or AAV8-shRNA-*SAA1/2* and further fed by a HFD for 10 weeks. (**A**) Schematic of the experimental design of AAV8-shRNA treatment in HFD-mice model. (**B**) Plasma concentrations of SAA from mice treated with AAV8-shRNA-sc or AAV8-shRNA-*SAA1/2* (n = 10). (**C**) Body weight during 16 weeks HFD feeding (n = 10). (**D**) Fasting blood glucose in mice (n = 10). (**E, F**) GTT (E) and ITT (F) in mice (n = 7). (**G, H**) Representative images (G) and quantifications (H) of F4/80-positive macrophages area of representative liver sections (n = 6). Scale bar, 20 μm. (**I**) mRNA levels of inflammatory mediators in the liver of HFD-fed mice (n = 11–12). (**J**) TG (left) and TCH (right) levels in the plasma of HFD-fed mice (n = 10). (**K**) The liver weights of AAV8-shRNA-*SAA1/2* mice and controls at 16 weeks post-HFD administration (n = 10). (**L**) Liver TG (left) and TCH (right) levels in mice (n = 10). (**M**) Representative images showing H&E staining (top) and Oil Red O staining (bottom) of liver sections of mice. Scale bar, 50 μm. (**N**) Quantifications of lipid droplet area in Oil Red O staining of representative liver sections (n = 6). (**O**) Plasma levels of ALT in mice (n = 10). All data are expressed as means ± SEMs. *P < 0.05, **P < 0.01, ***P < 0.001. (For interpretation of the references to color in this figure legend, the reader is referred to the Web version of this article.)

SAA1 is recognized by several receptors including formyl peptide receptor like 1 (FPRL1), TLRs and scavenger receptor B (SR-B) [30,41–43]. In general, the mature SAA1 pro-inflammatory signaling relies on the TLR2 or TLR4 in target cells [38]. We demonstrated that TLR4 signaling was necessity for SAA1-induced hepatic steatosis and inflammation in HFD-fed mice. Binding of SAA1 with TLR4 and MD2 induced internalization of TLR4. It is intrigued that the SAA1-induced TLR4 internalization seems not rely on dimerization of the TLR4-MD2 complex as LPS, a canonical TLR4 agonist, does. Consistently, Jeong et al. has reported that PA binds with a monomeric TLR4-MD2 complex triggering endocytosis and pro-IL-1β expression in macrophages [26]. Of note, both SAA1 and PA are endogenous damage-associated molecular patterns (DAMP) those are distinctive from LPS, a gram-negative related prototypical pathogen-associated molecular patterns (PAMP). With four antiparallel helices [44], SAA1 may activate TLR4 signaling in a not yet identified mechanism in hepatocytes which warrants further structural biological investigations.

The finding that upregulated SAA1 was only in the HFD-fed murine liver but not in other TLR4-expressed tissues including epiWAT, muscle and heart indicates the importance of the liver in the SAA1's action. However, the possibility that SAA1 autocrine occurs in other tissues is not ruled out because SAA1 is a hepatokine and TLR4 is widely expressed in hepatocytes and other cells [45,46]. Importantly, identification of autocrine regulatory mechanism of SAA1 does not only partly explain its increased expression in the fatty liver. After promoting hepatic lipid accumulation, the SAA1-induced chronic inflammation strikes the fat-laden or damaged hepatocytes and drives NAFLD progression. It has been reported that inflammation promotes sustained hepatic fibrogenesis, which ultimately leads to cirrhosis [33]. Inflammation also probably precedes NASH contributing to pathophysiological mechanism inducing liver fibrosis [47]. Although accumulative lines of evidence support the concept that hepatic inflammation drives liver fibrosis, the prognostic relevance and therapeutic target of inflammation in NAFLD are still open issues. For example, anti-inflammatory therapies such as CCR2/5 inhibitor cenicriviroc and apoptosis signal-regulating kinase 1 (ASK1) inhibitor selonsertib have met challenges in clinical practice with limited therapeutic effects and side effects [48,49]. Administration of hyperlipidemic mice by AAV8-shRNA-*SAA1/2* alleviating the NAFLD-related phenotype supports the notion that SAA1/TLR4/NF-κB/SAA1 positive feedback in hepatocytes may be a potential target for therapy by antagonizing hepatic steatosis and inflammation. In summary, we identify that SAA1 acts as a critical hepatokine promoting the progression of fatty liver, which confers it as a potential therapeutic target for obesity-associated NAFLD.

CONTRIBUTION STATEMENT

Q Chen, J Ben and X Yang conceived and designed the work. B Jiang, D Wang, Y Hu, W Li, F Liu performed research, collected and analyzed the data. J Ben, X Zhu, X Li, H Zhang, H Bai and Q Yang provided technical assistance. B Jiang, D Wang, J Ben and Q Chen wrote the paper. All authors read and approved the final manuscript.

DATA AVAILABILITY

The data are available from the corresponding author on reasonable request.

ACKNOWLEDGEMENTS

This work was supported by grants from the National Natural Science Foundation of China (Nos. 81830011, 82030012 to Q Chen; Nos. 81870371, 82070457 to J Ben; Nos. 82100433 to B Jiang; No. 81770417 to X Zhu; No. 81670263 to X Li), the Natural Science Foundation of the Jiangsu Higher Education Institutions of China (18KJA310003 to J Ben; 20KJA310007 to X.Z.).

CONFLICT OF INTEREST

None declared.

APPENDIX A. SUPPLEMENTARY DATA

Supplementary data to this article can be found online at https://doi.org/10.1016/j.molmet.2022.101462.

REFERENCES

[1] Eslam, M., Sanyal, A.J., George, J., 2020. MAFLD: a consensus-driven proposed nomenclature for metabolic associated fatty liver disease. Gastroenterology 158(7):1999–2014. https://doi.org/10.1053/j.gastro.2019.11.312 e1991.

[2] Younossi, Z., Tacke, F., Arrese, M., Chander Sharma, B., Mostafa, I., Bugianesi, E., et al., 2019. Global perspectives on nonalcoholic fatty liver disease and nonalcoholic steatohepatitis. Hepatology 69(6):2672–2682. https://doi.org/10.1002/hep.30251.

[3] Hardy, T., Oakley, F., Anstee, Q.M., Day, C.P., 2016. Nonalcoholic fatty liver disease: pathogenesis and disease spectrum. Annual Review of Pathology 11: 451–496. https://doi.org/10.1146/annurev-pathol-012615-044224.

[4] Friedman, S.L., Neuschwander-Tetri, B.A., Rinella, M., Sanyal, A.J., 2018. Mechanisms of NAFLD development and therapeutic strategies. Nature Medicine 24(7):908–922. https://doi.org/10.1038/s41591-018-0104-9.

[5] Sanyal, A.J., 2019. Past, present and future perspectives in nonalcoholic fatty liver disease. Nature Reviews Gastroenterology & Hepatology 16(6):377–386. https://doi.org/10.1038/s41575-019-0144-8.

[6] Neuschwander-Tetri, B.A., 2010. Hepatic lipotoxicity and the pathogenesis of nonalcoholic steatohepatitis: the central role of nontriglyceride fatty acid metabolites. Hepatology 52(2):774–788. https://doi.org/10.1002/hep.23719.

[7] Younossi, Z., Anstee, Q.M., Marietti, M., Hardy, T., Henry, L., Eslam, M., et al., 2018. Global burden of NAFLD and NASH: trends, predictions, risk factors and prevention. Nature Reviews Gastroenterology & Hepatology 15(1):11–20. https://doi.org/10.1038/nrgastro.2017.109.

[8] Cai, J., Zhang, X.J., Li, H., 2018. Role of innate immune signaling in non-alcoholic fatty liver disease. Trends in Endocrinology and Metabolism: Trends in Endocrinology and Metabolism 29(10):712–722. https://doi.org/10.1016/j.tem.2018.08.003.

[9] Jia, L., Vianna, C.R., Fukuda, M., Berglund, E.D., Liu, C., Tao, C., et al., 2014. Hepatocyte Toll-like receptor 4 regulates obesity-induced inflammation and insulin resistance. Nature Communications 5:3878. https://doi.org/10.1038/ncomms4878.

[10] Sun, L., Ye, R.D., 2016. Serum amyloid A1: structure, function and gene polymorphism. Gene 583(1):48–57. https://doi.org/10.1016/j.gene.2016.02.044.

[11] Sack Jr., G.H., 2018. Serum amyloid A - a review. Molecular Medicine (Cambridge, Mass) 24(1):46. https://doi.org/10.1186/s10020-018-0047-0.

[12] Marzi, C., Huth, C., Herder, C., Baumert, J., Thorand, B., Rathmann, W., et al., 2013. Acute-phase serum amyloid A protein and its implication in the development of type 2 diabetes in the KORA S4/F4 study. Diabetes Care 36(5):1321–1326. https://doi.org/10.2337/dc12-1514.

[13] de Oliveira, E.M., Ascar, T.P., Silva, J.C., Sandri, S., Migliorini, S., Fock, R.A., et al., 2016. Serum amyloid A links endotoxaemia to weight gain and insulin resistance in mice. Diabetologia 59(8):1760—1768. https://doi.org/10.1007/s00125-016-3970-z.

[14] Wang, Y., Cao, F., Wang, Y., Yu, G., Jia, B.L., 2019. Silencing of SAA1 inhibits palmitate- or high-fat diet induced insulin resistance through suppression of the NF-κB pathway. Molecular Medicine (Cambridge, Mass) 25(1):17. https://doi.org/10.1186/s10020-019-0075-4.

[15] Neuman, G., Sagi, R., Shalitin, S., Reif, S., 2010. Serum inflammatory markers in overweight children and adolescents with non-alcoholic fatty liver disease. The Israel Medical Association Journal : The Israel Medical Association Journal 12(7):410—415.

[16] Yuan, Z.Y., Zhang, X.X., Wu, Y.J., Zeng, Z.P., She, W.M., Chen, S.Y., et al., 2019. Serum amyloid A levels in patients with liver diseases. World Journal of Gastroenterology 25(43):6440—6450. https://doi.org/10.3748/wjg.v25.i43.6440.

[17] Li, D., Xie, P., Zhao, S., Zhao, J., Yao, Y., Zhao, Y., et al., 2021. Hepatocytes derived increased SAA1 promotes intrahepatic platelet aggregation and aggravates liver inflammation in NAFLD. Biochemical and Biophysical Research Communications 555:54—60. https://doi.org/10.1016/j.bbrc.2021.02.124.

[18] Lee, J.Y., Hall, J.A., Kroehling, L., Wu, L., Najar, T., Nguyen, H.H., et al., 2020. Serum amyloid A proteins induce pathogenic Th17 cells and promote inflammatory disease. Cell 180(1):79—91. https://doi.org/10.1016/j.cell.2019.11.026 e16.

[19] Ather, J.L., Ckless, K., Martin, R., Foley, K.L., Suratt, B.T., Boyson, J.E., et al., 2011. Serum amyloid A activates the NLRP3 inflammasome and promotes Th17 allergic asthma in mice. The Journal of Immunology 187(1):64—73. https://doi.org/10.4049/jimmunol.1100500 (Baltimore, Md : 1950).

[20] Lee, H.Y., Kim, S.D., Shim, J.W., Lee, S.Y., Lee, H., Cho, K.H., et al., 2008. Serum amyloid A induces CCL2 production via formyl peptide receptor-like 1-mediated signaling in human monocytes. The Journal of Immunology 181(6):4332—4339. https://doi.org/10.4049/jimmunol.181.6.4332 (Baltimore, Md : 1950).

[21] Liu, D., Zhang, P., Zhou, J., Liao, R., Che, Y., Gao, M.M., et al., 2020. TNFAIP3 interacting protein 3 overexpression suppresses nonalcoholic steatohepatitis by blocking TAK1 activation. Cell Metabolism 31(4):726—740. https://doi.org/10.1016/j.cmet.2020.03.007 e728.

[22] Chalasani, N., Younossi, Z., Lavine, J.E., Charlton, M., Cusi, K., Rinella, M., et al., 2018. The diagnosis and management of nonalcoholic fatty liver disease: practice guidance from the American Association for the Study of Liver Diseases. Hepatology 67(1):328—357. https://doi.org/10.1002/hep.29367.

[23] Park, B.S., Song, D.H., Kim, H.M., Choi, B.S., Lee, H., Lee, J.O., 2009. The structural basis of lipopolysaccharide recognition by the TLR4-MD-2 complex. Nature 458(7242):1191—1195. https://doi.org/10.1038/nature07830.

[24] Ben, J., Jiang, B., Wang, D., Liu, Q., Zhang, Y., Qi, Y., et al., 2019. Major vault protein suppresses obesity and atherosclerosis through inhibiting IKK-NF-κB signaling mediated inflammation. Nature Communications 10(1):1801. https://doi.org/10.1038/s41467-019-09588-x.

[25] Zanoni, I., Ostuni, R., Marek, L.R., Barresi, S., Barbalat, R., Barton, G.M., et al., 2011. CD14 controls the LPS-induced endocytosis of Toll-like receptor 4. Cell 147(4):868—880. https://doi.org/10.1016/j.cell.2011.09.051.

[26] Kim, S.Y., Jeong, J.M., Kim, S.J., Seo, W., Kim, M.H., Choi, W.M., et al., 2017. Pro-inflammatory hepatic macrophages generate ROS through NADPH oxidase 2 via endocytosis of monomeric TLR4-MD2 complex. Nature Communications 8(1):2247. https://doi.org/10.1038/s41467-017-02325-2.

[27] Lefebvre, P., Lalloyer, F., Baugé, E., Pawlak, M., Gheeraert, C., Dehondt, H., et al., 2017. Interspecies NASH disease activity whole-genome profiling identifies a fibrogenic role of PPARα-regulated dermatopontin. JCI Insight 2(13). https://doi.org/10.1172/jci.insight.92264.

[28] Zhang, X., Shen, J., Man, K., Chu, E.S., Yau, T.O., Sung, J.C., et al., 2014. CXCL10 plays a key role as an inflammatory mediator and a non-invasive biomarker of non-alcoholic steatohepatitis. Journal of Hepatology 61(6):1365—1375. https://doi.org/10.1016/j.jhep.2014.07.006.

[29] Dali-Youcef, N., Vix, M., Costantino, F., El-Saghire, H., Lhermitte, B., Callari, C., et al., 2019. Interleukin-32 contributes to human nonalcoholic fatty liver disease and insulin resistance. Hepatology Communications 3(9):1205—1220. https://doi.org/10.1002/hep4.1396.

[30] Sandri, S., Rodriguez, D., Gomes, E., Monteiro, H.P., Russo, M., Campa, A., 2008. Is serum amyloid A an endogenous TLR4 agonist? Journal of Leukocyte Biology 83(5):1174—1180 https://doi.org/10.1189/jlb.0407203.

[31] Ryu, S.J., Park, S.C., 2009. Targeting major vault protein in senescence-associated apoptosis resistance. Expert Opinion on Therapeutic Targets 13(4):479—484. https://doi.org/10.1517/14728220902832705.

[32] Lee, Y.A., Wallace, M.C., Friedman, S.L., 2015. Pathobiology of liver fibrosis: a translational success story. Gut 64(5):830—841. https://doi.org/10.1136/gutjnl-2014-306842.

[33] Koyama, Y., Brenner, D.A., 2017. Liver inflammation and fibrosis. Journal of Clinical Investigation 127(1):55—64. https://doi.org/10.1172/jci88881.

[34] Liu, L.R., Lin, S.P., Chen, C.C., Chen, Y.J., Tai, C.C., Chang, S.C., et al., 2011. Serum amyloid A induces lipolysis by downregulating perilipin through ERK1/2 and PKA signaling pathways. Obesity 19(12):2301—2309. https://doi.org/10.1038/oby.2011.176.

[35] Yu, C.J., Wang, Q.S., Wu, M.M., Song, B.L., Liang, C., Lou, J., et al., 2018. TRUSS exacerbates NAFLD development by promoting IκBα degradation in mice. Hepatology 68(5):1769—1785. https://doi.org/10.1002/hep.30066.

[36] Xu, M., Ge, C., Zhu, L., Qin, Y., Du, C., Lou, D., et al., 2021. iRhom2 promotes hepatic steatosis by activating MAP3K7-dependent pathway. Hepatology 73(4):1346—1364. https://doi.org/10.1002/hep.31436.

[37] De Buck, M., Gouwy, M., Wang, J.M., Van Snick, J., Proost, P., Struyf, S., et al., 2016. The cytokine-serum amyloid A-chemokine network. Cytokine & Growth Factor Reviews 30:55—69. https://doi.org/10.1016/j.cytogfr.2015.12.010.

[38] Ye, R.D., Sun, L., 2015. Emerging functions of serum amyloid A in inflammation. Journal of Leukocyte Biology 98(6):923—929. https://doi.org/10.1189/jlb.3VMR0315-080R.

[39] Cheng, N., Liang, Y., Du, X., Ye, R.D., 2018. Serum amyloid A promotes LPS clearance and suppresses LPS-induced inflammation and tissue injury. EMBO Reports 19(10). https://doi.org/10.15252/embr.201745517.

[40] Kim, M.H., de Beer, M.C., Wroblewski, J.M., Webb, N.R., de Beer, F.C., 2013. SAA does not induce cytokine production in physiological conditions. Cytokine 61(2):506—512. https://doi.org/10.1016/j.cyto.2012.10.019.

[41] Su, S.B., Gong, W., Gao, J.L., Shen, W., Murphy, P.M., Oppenheim, J.J., et al., 1999. A seven-transmembrane, G protein-coupled receptor, FPRL1, mediates the chemotactic activity of serum amyloid A for human phagocytic cells. Journal of Experimental Medicine 189(2):395—402. https://doi.org/10.1084/jem.189.2.395.

[42] Cai, L., de Beer, M.C., de Beer, F.C., van der Westhuyzen, D.R., 2005. Serum amyloid A is a ligand for scavenger receptor class B type I and inhibits high density lipoprotein binding and selective lipid uptake. Journal of Biological Chemistry 280(4):2954—2961. https://doi.org/10.1074/jbc.M411555200.

[43] Cheng, N., He, R., Tian, J., Ye, P.P., Ye, R.D., 2008. Cutting edge: TLR2 is a functional receptor for acute-phase serum amyloid A. The Journal of Immunology 181(1):22—26. https://doi.org/10.4049/jimmunol.181.1.22 (Baltimore, Md : 1950).

[44] Lu, J., Yu, Y., Zhu, I., Cheng, Y., Sun, P.D., 2014. Structural mechanism of serum amyloid A-mediated inflammatory amyloidosis. Proceedings of the National Academy of Sciences of the United States of America 111(14):5189—5194. https://doi.org/10.1073/pnas.1322357111.

[45] Frantz, S., Kobzik, L., Kim, Y.D., Fukazawa, R., Medzhitov, R., Lee, R.T., et al., 1999. Toll4 (TLR4) expression in cardiac myocytes in normal and failing myocardium. Journal of Clinical Investigation 104(3):271—280. https://doi.org/10.1172/jci6709.

[46] Lin, Y., Lee, H., Berg, A.H., Lisanti, M.P., Shapiro, L., Scherer, P.E., 2000. The lipopolysaccharide-activated toll-like receptor (TLR)-4 induces synthesis of the closely related receptor TLR-2 in adipocytes. Journal of Biological Chemistry 275(32):24255–24263. https://doi.org/10.1074/jbc.M002137200.

[47] Filozof, C., Chow, S.C., Dimick-Santos, L., Chen, Y.F., Williams, R.N., Goldstein, B.J., et al., 2017. Clinical endpoints and adaptive clinical trials in precirrhotic nonalcoholic steatohepatitis: facilitating development approaches for an emerging epidemic. Hepatology Communications 1(7):577–585. https://doi.org/10.1002/hep4.1079.

[48] Friedman, S., Sanyal, A., Goodman, Z., Lefebvre, E., Gottwald, M., Fischer, L., et al., 2016. Efficacy and safety study of cenicriviroc for the treatment of non-alcoholic steatohepatitis in adult subjects with liver fibrosis: CENTAUR Phase 2b study design. Contemporary Clinical Trials 47: 356–365. https://doi.org/10.1016/j.cct.2016.02.012.

[49] Younossi, Z.M., Stepanova, M., Lawitz, E., Charlton, M., Loomba, R., Myers, R.P., et al., 2018. Improvement of hepatic fibrosis and patient-reported outcomes in non-alcoholic steatohepatitis treated with selonsertib. Liver International : Official Journal of the International Association for the Study of the Liver 38(10):1849–1859. https://doi.org/10.1111/liv.13706.

